

SCIENTIFIC REPORTS



OPEN

Enhanced Performance of PbS-quantum-dot-sensitized Solar Cells via Optimizing Precursor Solution and Electrolytes

Received: 04 March 2015
Accepted: 25 February 2016
Published: 15 March 2016

Jianjun Tian¹, Ting Shen¹, Xiaoguang Liu¹, Chengbin Fei², Lili Lv¹ & Guozhong Cao^{2,3}

This work reports a PbS-quantum-dot-sensitized solar cell (QDSC) with power conversion efficiency (PCE) of 4%. PbS quantum dots (QDs) were grown on mesoporous TiO₂ film using a successive ion layer absorption and reaction (SILAR) method. The growth of QDs was found to be profoundly affected by the concentration of the precursor solution. At low concentrations, the rate-limiting factor of the crystal growth was the adsorption of the precursor ions, and the surface growth of the crystal became the limiting factor in the high concentration solution. The optimal concentration of precursor solution with respect to the quantity and size of synthesized QDs was 0.06 M. To further increase the performance of QDSCs, the 30% deionized water of polysulfide electrolyte was replaced with methanol to improve the wettability and permeability of electrolytes in the TiO₂ film, which accelerated the redox couple diffusion in the electrolyte solution and improved charge transfer at the interfaces between photoanodes and electrolytes. The stability of PbS QDs in the electrolyte was also improved by methanol to reduce the charge recombination and prolong the electron lifetime. As a result, the PCE of QDSC was increased to 4.01%.

Like other traditional photovoltaics, p-n junction crystalline silicon (c-Si) solar cells are costly to manufacture and install. Developing highly efficient solar cells that would be economically viable is becoming an increasingly urgent task imposed on the scientists around the world^{1,2}. Semiconductor quantum dots (QDs) are solution-processable semiconductor nanocrystals, and they have been recognized as a suitable material for next-generation solar cells due to their versatile optical and electrical properties^{3–5}. Recently, QDs have been used in photovoltaics to form quantum dots solar cells (QDSCs) for the following reasons: (1) tunable band gap depending on QD size, (2) large extinction coefficient, (3) stability toward water and oxygen, and (4) multiple exciton generation (MEG) with single-photon absorption^{6–8}. The theoretical power conversion efficiency (PCE) of QDSCs can reach up to 42% in view of MEG effect of QDs, which is much higher than that of semiconductor solar cells (31%) according to Shockley-Queisser limit^{9–11}.

Among the various QDs, CdS, and CdSe are usually used for QDSCs because of their high potential for light harvesting in the visible light region^{12,13}. In addition, CdS can be used to induce CdS/CdSe co-sensitization, which broadens the optical absorption of QDs and increases the efficiency of the solar cells. Recently, a CdS/CdSe QDSC with efficiency of 6.33% was prepared by doping Mn²⁺ into CdSe¹⁴. Kamat *et al.* reported a PCE of 6.6% CdS/CdSe QDSC after the introduction of a layer of Cu_xS on the surface of CdSe QDs¹⁵. However, CdSe has a band gap (E_g) of 1.7 eV and may absorb photons with wavelengths shorter than 700 nm¹⁶. Using these QDs (E_g > 1.5 eV), it may not be possible to utilize the full solar spectrum, which limits improvement of the photo-current density and PCE of the solar cells¹⁷. Low-E_g (< 1.5 eV) QDs have shown considerable potential for the QDSCs with high photo-generated current density and PCE attributable to near infrared (IR) absorption. PbS is one of the most intensively studied low E_g semiconductors, with an E_g in the near IR region of 0.41 eV^{17,18}. PbS also has a high absorption coefficient of 1–5 × 10⁵ cm⁻¹ and Bohr excitation radius of 18 nm^{19,20}. In this way, PbS QDs is an ideal sensitizer for QDSCs. However, PbS-sensitized solar cells are much less efficient than CdS/CdSe

¹Institute of Advanced Materials and Technology, University of Science and Technology Beijing, Beijing, 100083, China. ²Beijing Institute of Nanoenergy and Nanosystems, Chinese Academy of Sciences, 100083, China. ³Department of Materials and Engineering, University of Washington, Seattle, WA, 98195-2120, USA. Correspondence and requests for materials should be addressed to J.T. (email: tianjianjun@mater.ustb.edu.cn)

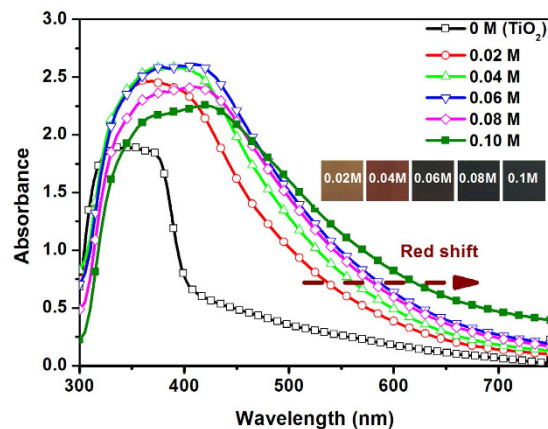


Figure 1. UV-visible spectra curves of the bare TiO_2 film and TiO_2 films loaded with PbS QDs from precursor solutions of different concentrations; inset shows the color of the film.

QDSCs, no more than 4% without co-sensitization or doping. A great deal of effort has been made to enhance the PCE of QDSCs^{18,21–23}. Mora-Seró *et al.* developed a CdS coating layer that could be added to the surface of PbS to produce PbS-CdS co-sensitized solar cells¹⁸. The PCE of the solar cells exceeded 4%. N.G. Park *et al.* reported a highest PCE of 5.6% for another set of solar cells, which was produced by doping Hg into PbS¹⁷. Without using co-sensitization or doping, the highest PCE of any solar cell was 3.6%, and it was reported by Loiudice and Rizzo²⁴. To date, the PCE of PbS QDSCs do not reach expectations. This may be because of the high charge recombination of the solar cells and instability of PbS in the electrolyte^{18,21,25}. To solve these problems, research should focus on controlling the synthesis process for QDs of suitable quantity and size, and optimizing the electrolyte solution to improve their stability.

In a typical fabrication of QDSC photoanodes, QDs are deposited directly onto the oxide anode in the precursor solutions^{9,26}. These approaches, including chemical bath deposition (CBD)²⁷ and successive ionic layer adsorption and reaction (SILAR)^{28,29}, have shown good performance because of the close contact between QDs and oxide anodes. CBD is a relatively simple method of depositing QDs and nanoparticles. It has many advantages, such as stable yield, robust adherence and good reproducibility. The growth of QDs is heavily dependent on the growth conditions, such as the duration of deposition, the composition and temperature of the solution, and the characteristics of the anode films³⁰. At present, CBD is rarely used in the fabrication of PbS QDs for the solar cells. The SILAR method is based on successive reactions on the surface of oxides. Each reaction is followed by rinsing, which facilitates a heterogeneous reaction between the solid phase and the solvated ions in the solution³⁰. The mechanism underlying SILAR shows that the number and sizes of adsorbed QDs affect the performance of QDSCs. These factors have a close relationship with the concentration and composition of the precursor solution. Although the SILAR is widely used in PbS-based QDSCs, there are few studies on the mechanism underlying the relationship between PbS growth and the concentration of the precursor solution. Here, the SILAR approach was used for the fabrication of PbS QDs, and the growth, quantity, and size of PbS QDs were studied. In addition, to improve the diffusion and wettability of the electrolyte in the mesoporous oxide film, 30% of the deionized water of polysulfide electrolyte was replaced with methanol. The stability of PbS in the electrolyte was also improved by adding methanol. Results showed that the solar cells could be optimized by adjusting precursor concentration and electrolyte, producing PCEs of up to 4.01%.

Results

PbS QDs were directly deposited on mesoporous TiO_2 films using successive ionic layer adsorption and reaction (SILAR). The concentration of the precursor solution was found to be a key factor affecting the quantities and particle size of QDs. Although there are no ideal measurements that can be used to estimate the numbers and particle sizes of PbS within the film accurately because of the low mass fraction and very small size of QDs, the effects of the concentration can be deduced by measuring the changes in the light absorbance of film loaded with PbS QDs. Figure 1 displays the UV-visible spectra curves of the bare TiO_2 film and the films loaded with PbS QDs deposited from precursor solutions with different concentrations. It is clear that both absorbance and absorption range of the TiO_2 film are increased by loading PbS QDs. In addition, the absorbance of the films increases as the increase of concentration, and peaks at a concentration of 0.06 M. However, when the concentration is increased further, the absorbance of the film decreases. The number of QDs is proportional to the absorbance of the film with loading of QDs. For this reason, the highest number of QDs is synthesized in 0.06 M precursor solution. As shown in the inset of Fig. 1, the films gradually darken as the concentration increased. When the concentration of the solution reaches 0.06 M, the film is entirely black. As shown in Fig. 1, results also show that the absorption edges of the film loaded with PbS QDs shift towards long wavelengths as the concentration increased (red shift), which causes a decrease in the band gap (E_g). The decrease in E_g is caused by increases in the size of QDs (quantum size effect). The PbS QDs increased in size as concentration increased. To understand the relationship between the concentration and optical absorption properties of QDs, the formation and growth of QDs should be discussed further.

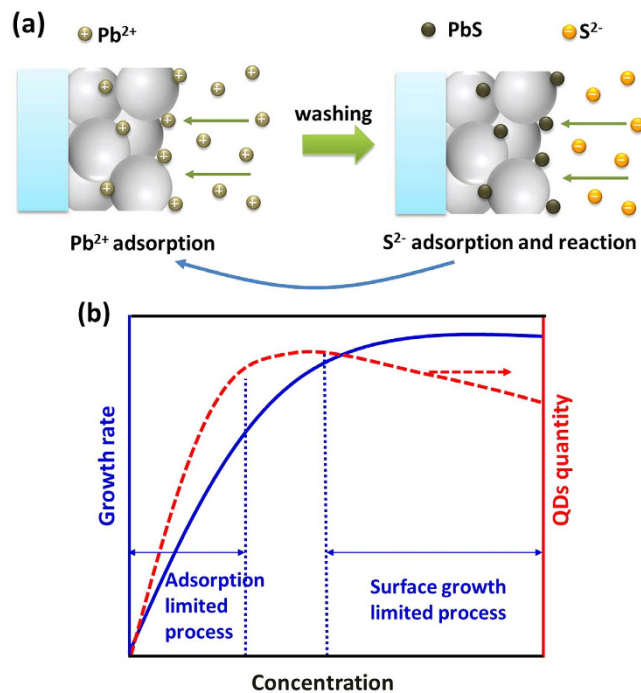


Figure 2. (a) Schematic synthesis of PbS QDs using the SILAR method and (b) the effect of precursor concentration on the growth rate and quantity of PbS QDs. It is derived from the findings of a previous study³¹.

Figure 2(a) shows the synthesis of PbS QDs using the SILAR method. Pb²⁺ ions are adsorbed onto the surface of oxide (TiO₂) nanoparticles during the first dipping step in the metallic precursor solution. After the washing, Pb²⁺ reacts with S²⁻ to form PbS QDs on the TiO₂ surface at the second dipping step in the sulfur precursor solution. When a new phase forms on the surface of another material, the process is called heterogeneous nucleation³¹. Figure 2(a) shows that the formation of PbS QDs involves heterogeneous nucleation. After nucleation, PbS crystals grow quickly. Crystal growth can be generally considered a heterogeneous reaction. The concentration of the precursor solution is key factor for the growth rate. Figure 2(b) shows the effect of the concentration on the growth rate of PbS QDs. This effect is derived from the findings of a previous study according to the fundamentals of heterogeneous nucleation and crystal growth³¹. When the concentration of the precursor solution is low, the adsorption of ions acts as a rate-limiting factor for crystal growth. For a given system, the growth rate of the crystal increases with the increase of the concentration in a linear fashion. Further increases in the concentration can cause a change in the limiting factor from the adsorption of ions to the surface growth of the crystal. When the surface growth becomes a limiting factor, the growth rate of the crystals becomes independent of the concentration. As shown in Fig. 2(b), when the adsorption of ions is the limiting factor, both the number of QDs and particle size increase as the concentration of the precursor solution increases because more ions can be adsorbed accordingly. When the concentration exceeds 0.06 M, the number of ions adsorbed reaches saturation and the surface growth become the limiting factor. The number of ions adsorbed does not increase with further increases in concentration. However, the crystals still increase in size. These large crystals can block some interior pores, which reduces the number of adsorbed ions. The number of PbS QDs decreases slightly, which is closely consistent with the results of UV-visible absorbance.

Figure 3 shows the TEM micrographs of bare TiO₂ nanoparticles and PbS QDs adsorbed TiO₂ nanoparticles prepared using precursor solutions of different concentrations. The TEM samples were selected from the small TiO₂ nanoparticles adsorbed with PbS QDs, which were suspended in the ethanol. Although TEM is not an ideal approach to determining the size and number of PbS QDs at the different precursor solution concentrations, it can serve as a suitable supplementary method. The results recorded here clearly show that semi-spherical QDs form only sparsely on the surfaces of TiO₂ nanoparticles. Both the number and size of QDs increase with increasing precursor solution concentration. The average size of QDs is calculated by statistical analysis of TEM images. The average sizes of QDs are 2.44 ± 0.23 nm for Fig. 3(b), 3.93 ± 0.27 nm for Fig. 3(c), 4.72 ± 0.31 nm for Fig. 3(d), 4.93 ± 0.34 nm for Fig. 3(e) and 5.36 ± 0.38 nm for Fig. 3(f), respectively. The concentration exceeds 0.06 M, and the size and number of QDs show no obvious change, which is consistent with findings shown in Fig. 2(b). However, the concentration of precursor solution is increased further (up to 0.1 M), QDs are easy to aggregate, which blocks the holes and pores among the TiO₂ nanoparticles as shown in Fig. 3(f). The aggregation of QDs will reduce the PCE of the solar cell due to high surface charge recombination. In addition, the size of the PbS QDs is an important parameter that may regulate charge injection. According to results reported by Braga *et al.*³² and Concina *et al.*³³, the conduction band (CB) of bulk PbS is lower than that of TiO₂, which suppresses electron injection from PbS into TiO₂. This problem can be solved by reducing the size of PbS particles to below the Bohr's radius due to the quantum confinement. The energy position of CB is up-shifted by decreasing the size of PbS. So the fast

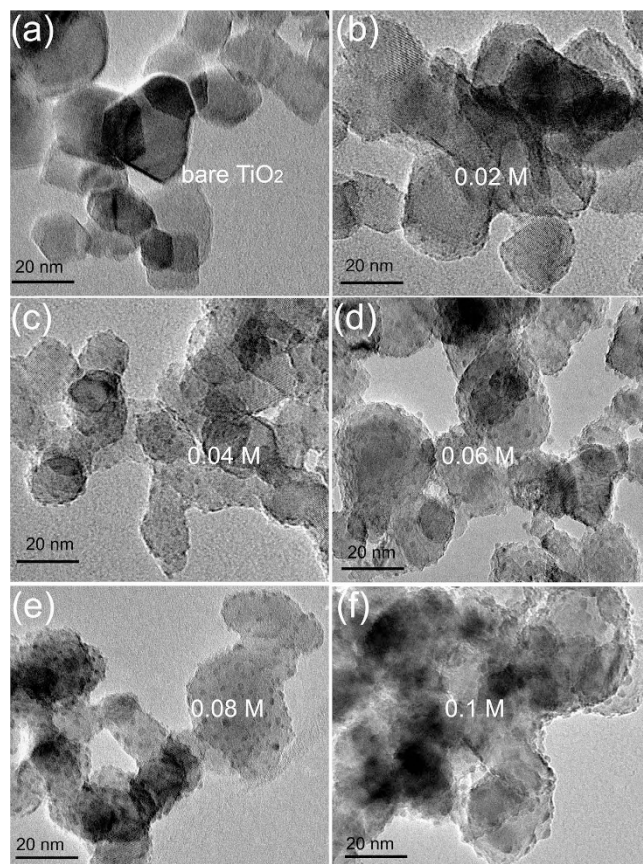


Figure 3. TEM images of (a) bare TiO₂ film, and TiO₂ film loaded with PbS QDs from precursor solutions of different concentrations (b) 0.02 M, (c) 0.04 M, (d) 0.06 M, (e) 0.08 M and (f) 0.1 M.

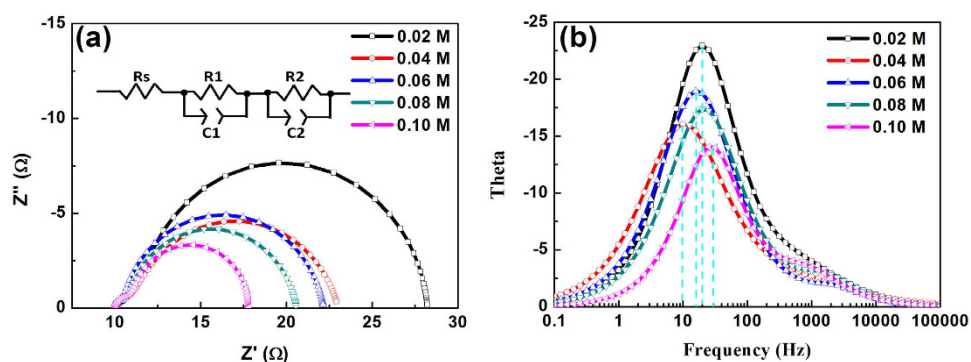


Figure 4. (a) Nyquist plot and (b) Bode plot curves of the QDSCs under light intensity, 100 mW/cm².

electrons can transfer from PbS into TiO₂. However, very small QDs have many more surface defects, which cause high surface charge recombination. For this reason, PbS QDs should be neither too large nor too small.

Figure 4 shows the electrochemical impedance spectra (EIS) of QDSCs under the light intensity of 100 mW/cm². The fitting results of the impedance spectra are listed in Table 1. Under illumination, the solar cell can be considered a diode^{34–37}. As shown in Fig. 4(a), the hemisphere in the high-frequency region (10¹–10² Hz) represents the resistance of charge transport at the counter electrode/electrolyte interface (R₁). At low frequencies, the impedance related to the charge transport at the TiO₂/PbS/electrolyte interface can be described using R₂. The lower R₂ is, the faster the charge transfer and transport at the TiO₂/PbS/electrolyte interface is. The present work is focused mainly on the R₂, which shows the effect of precursor solution concentration on the charge transfer and transport at the TiO₂/PbS/electrolyte interfaces. Results show that R₂ decreases gradually with increasing precursor concentration. This is probably due to the increase in the number and size of QDs. In this way, the charge transport is sped up by increasing the concentration of the precursor solution, which facilitates charge collection for a high photo-current density of the solar cell. However, R₂ is also considered as a resistance of charge recombination

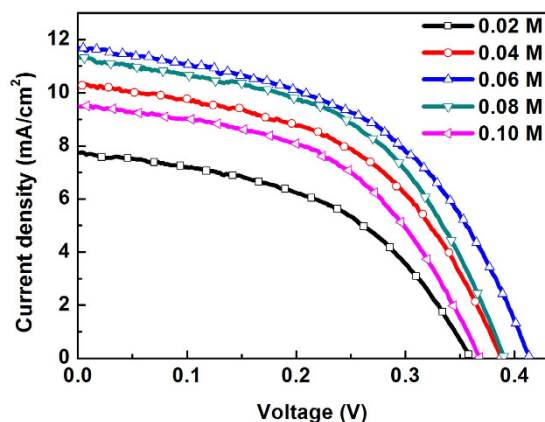


Figure 5. Photocurrent density-voltage (J-V) curves of QDSCs measured under AM 1.5 G, at 1 sunlight intensity.

Concentration (M)	$R_1(\Omega)$	$R_2(\Omega)$	τ_n (mS)
0.02	1.5 ± 0.4	16.7 ± 0.7	8.0 ± 0.5
0.04	1.1 ± 0.2	11.9 ± 0.5	12.6 ± 0.9
0.06	0.4 ± 0.1	11.8 ± 0.7	10.1 ± 0.9
0.08	0.7 ± 0.1	9.9 ± 0.4	8.0 ± 0.8
0.10	1.1 ± 0.2	6.8 ± 0.4	6.3 ± 0.6

Table 1. Electrochemical impedance results of QDSCs^a. ^aThe standard deviation of the properties is based on the statistical data of five cells.

Concentration (M)	V_{oc} (V)	J_{sc} (mA/cm ²)	FF(%)	PCE(%)
0.02	0.36 ± 0.01	7.44 ± 0.23	48.40 ± 2.13	1.34 ± 0.10
0.04	0.39 ± 0.02	10.32 ± 0.31	49.46 ± 1.44	1.98 ± 0.13
0.06	0.41 ± 0.02	11.68 ± 0.36	49.86 ± 1.52	2.41 ± 0.12
0.08	0.39 ± 0.03	11.33 ± 0.32	50.64 ± 1.61	2.24 ± 0.11
0.10	0.37 ± 0.02	9.48 ± 0.41	50.14 ± 2.06	1.75 ± 0.13

Table 2. Photovoltaic properties of QDSCs from J-V curves^a. ^aThe standard deviation of the properties is based on the statistical data of five cells.

at the interfaces of TiO₂/QDs/electrolytes³⁸. Decreases in R_2 can boost the charge recombination and shorten electron lifetime, which causes the performance of the solar cell to deteriorate. Figure 4(b) shows the Bode plots of the QDSCs. The curve peak of the spectrum can be used to determine the electron lifetime according to the equation (1)³⁹.

$$\tau_n = 1/(2\pi f_{\min}) \quad (1)$$

Here, τ_n is the electron lifetime, f_{\min} is minimum frequency of the Bode plot curves. The corresponding results are listed in Table 1. As shown, τ_n increases as the concentration of the precursor solution increases. The τ_n is up to the maximum value (12.6 mS), when the concentration is 0.04 M. When the concentration exceeds 0.06 M, τ_n decreases visibly. This may be because of increases in charge recombination in high-concentration solutions (>0.06 M). According to the results of the electron transfer and lifetime, the appropriate precursor concentration is around 0.06 M, which is in consistent with the results of the absorbance (Fig. 1).

Figure 5 shows photocurrent density-voltage (J-V) characteristics of solar cells measured under the illumination of one sun (AM 1.5, 100 mW·cm⁻²). The performance parameters of the solar cells, including open circuit potential (V_{oc}), short circuit current density (J_{sc}), fill factor (FF), and power conversion efficiency (PCE), are listed in Table 2. As shown, all parameters of J_{sc} , V_{oc} , and PCE increase as the concentration of the precursor solution increases from 0.02 M to 0.06 M. The increase in J_{sc} is caused by increases in the number of PbS QDs, which cases more optical absorption and faster electron transfer. However, when the concentration increases further to 0.08 M, J_{sc} decreases slightly due to the decrease in light absorbance and electron collection. In view of the EIS results, the decrease in V_{oc} can be attributed mainly to the increased surface charge recombination and shortened electron lifetime. As a result, the highest PCE, 2.41%, is obtained when the concentration of the precursor solution is 0.06 M.

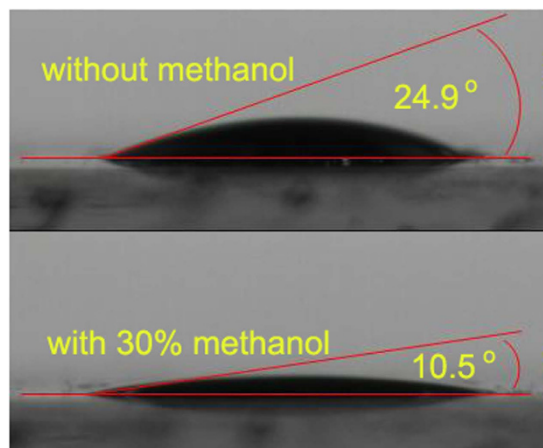


Figure 6. Contact angle images showing the wettability of the electrolyte with and without methanol.

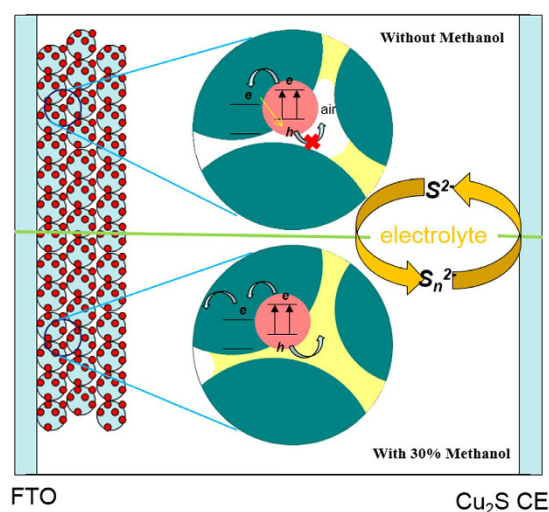


Figure 7. Schematic of the wettability and diffusion of different electrolytes.

To improve the wettability and penetrability of the electrolyte, methanol was replaced with 30% deionized water of polysulfide. As shown in Fig. 6, the contact angle of the electrolyte with methanol is 10.5° , which is much smaller than that of the electrolyte without methanol (24.9°). The smaller the contact angle is, the better the wettability of the electrolyte is. Figure 7 shows an illustration of the wettability and diffusion of the different electrolytes. Because there are a large number of adsorbed air molecules on the surface of TiO_2 nanoparticles, the interior pores of the film cannot be filled with the electrolyte solution. The improvement of wettability increases the penetrability of the electrolyte in the film, which is also helpful to the redox couple diffusion in the electrolyte and charge transport at the interfaces between photoanodes and electrolytes. In addition, PbS QDs is not stable in contact with polysulfide electrolyte, which decreases the photo-current density of the solar cell²⁵. The methanol in the electrolyte is found to improve the stability of PbS QDs in the electrolyte, and thus increase the photo-current density of the solar cell. To evaluate the properties of the electrolyte and stability of PbS in the electrolyte, the EIS of the solar cells should be studied further.

Figure 8 shows EIS curves of the QDSCs under a light intensity of 100 mW/cm^2 . As shown in Fig. 7(a), the R_2 of the solar cells using the electrolyte with 30% methanol is much lower than that of the one without methanol. It means that the electron transfer at the $\text{TiO}_2/\text{PbS}/\text{electrolyte}$ interface is accelerated by adding methanol to the electrolyte. The hemisphere in the low-frequency region (0.1–10 Hz) represents the diffusion impedance within the electrolyte⁴⁰. The improved electrolyte smaller value of R_3 than electrolyte without added methanol, indicating that the rate of diffusion of the redox couple in the electrolyte faster. As shown in Fig. 8(b), in the region of 0.1–1 Hz, there is an obvious peak in the red line Bode curve. This means that the improved electrolyte responds better to the change in frequency than the previous electrolyte. In this way, electron transfer and transport both at the interfaces and within the electrolyte solution can be improved by adding methanol to the electrolyte. In addition, the electron lifetime of the improved electrolyte is longer than that of the unmodified electrolyte in view of the peak of the Bode curve shift to low frequency. The increase in electron lifetime is derived from the decrease in the surface charge recombination, which can be attributed mainly to improvement in the stability of PbS in the

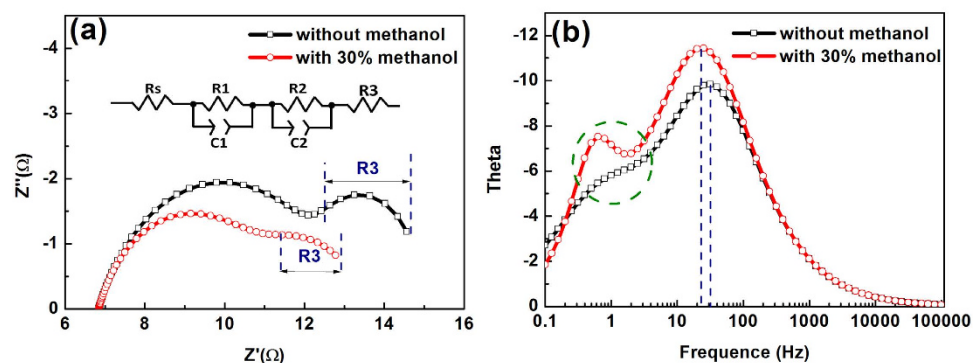


Figure 8. (a) Nyquist plot and (b) Bode plot curves of the QDSCs under light intensity, 100 mW/cm^2 .

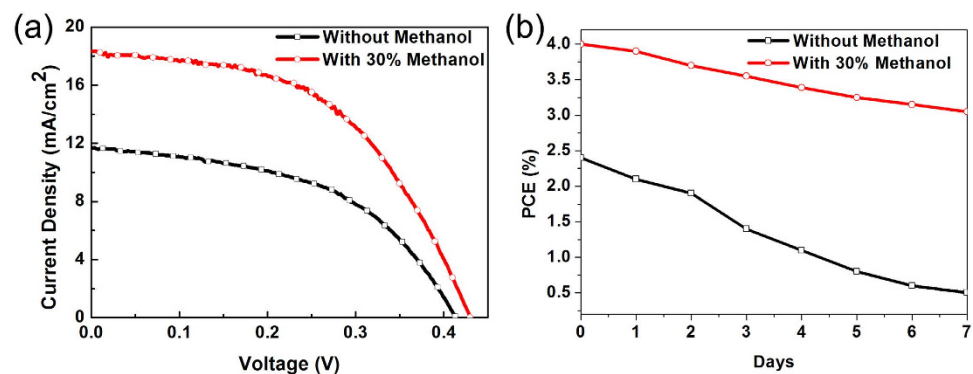


Figure 9. (a) Photocurrent density-voltage (J - V) curves of QDSCs measured under AM 1.5 G, at 1 sunlight intensity and (b) efficiency of QDSCs after different days when the sealed cells were exposed to air at 24°C .

Electrolyte	V_{oc} (V)	J_{sc} (mA/cm^2)	FF(%)	PCE(%)
Without methanol	0.41 ± 0.02	11.68 ± 0.36	49.86 ± 1.52	2.41 ± 0.12
With 30% methanol	0.43 ± 0.02	18.34 ± 0.42	50.86 ± 1.18	4.01 ± 0.16

Table 3. Photovoltaic properties of QDSCs from J - V curves^a. ^aThe standard deviation of the properties is based on the statistical data of five cells.

electrolyte. In addition, the methanol in the electrolyte solution may be involved in the redox reaction in the solar cell, which is another possible way to improve the performance of the device. However, it is very difficult to find evidence to support this conclusion.

Figure 9(a) shows photocurrent density-voltage (J - V) characteristics for the solar cells measured under the illumination of one sun (AM 1.5, $100 \text{ mW} \cdot \text{cm}^{-2}$). The performance parameters of the solar cells are listed in Table 3. The solar cell with the improved electrolyte exhibits a high performance: $J_{sc} = 18.34 \text{ mA/cm}^2$, $V_{oc} = 0.43$, $\text{FF} = 50.86\%$, $\text{PCE} = 4.01\%$. As shown, J_{sc} of the solar cell is visibly improved by adding methanol to the electrolyte, which is the main cause of improvement of the conversion efficiency. The remarkable increase in J_{sc} can be attributed to the improvement of PbS stability and to the enhancement of the transfer and lifetime of the electrons. Like J_{sc} , V_{oc} is increased by adding methanol to the electrolyte. This may have been due to the decrease in the charge recombination. As a result, the PCE of the solar cell is 66% higher than that of the solar cell made without added methanol (2.41%). The PCE recorded here, 4.01%, is one of the highest values for PbS-quantum-dot-sensitized solar cells without using co-sensitization or doping. In addition, the methanol in the electrolyte improved the stability of the solar cells as shown in Fig. 9(b).

Discussions

PbS quantum dots (QDs) were directly deposited onto the mesoporous TiO_2 film using the SILAR method. The process of formation of PbS QDs on the surfaces of TiO_2 nanoparticles is heterogeneous nucleation, which is visibly affected by the concentration of the precursor solution. The appropriate number and size of QDs within the TiO_2 film were determined when the concentration was 0.06 M. As the concentration of precursor solution increased further ($>0.06 \text{ M}$), the properties of QDSC started dropping due to the increase in surface charge recombination. To improve the wettability and penetrability of the electrolyte, the 30% deionized water of polysulfide electrolyte was replaced with methanol. The electrolyte not only accelerated the redox couple diffusion in

the electrolyte and the charge transfer at the interfaces between photoanodes and electrolyte but also enhanced the stability of PbS in the electrolyte to reduce the surface charge recombination. This produced a PCE of 4.01%, which is one of the highest values ever recorded for PbS QDSCs without co-sensitization or doping.

Methods

Preparation of mesoporous TiO₂ films. Mesoporous TiO₂ films with the thickness of 10 ± 0.5 μm were prepared via the doctor blading on the F:SnO₂ glass (FTO, 8 Ω/square) substrates using TiO₂ pastes mixed of TiO₂ nanoparticles (Degussa P25), ethyl cellulose and α-terpineol^{9,14}. The TiO₂ films underwent a sintering process in air at 500 °C for 30 min.

Fabrication of PbS QDs Sensitized Photoelectrodes. PbS QDs were deposited on the surface of TiO₂ films using successive ionic layer adsorption and reaction (SILAR) method. The mesoporous TiO₂ film was first dipped in a Pb(NO₃)₂ solution with solvent of deionized water and methanol as volume ratio of 1:1 for 1 min. Successively, the film was dipped into a Na₂S solution with solvent of deionized water and methanol as volume ratio of 1:1 for 1 min to allow S²⁻ to react with the preadsorbed Pb²⁺, leading to the formation of PbS. Between each dipping, the electrode was thoroughly washed with methanol. The sequence of dipping metallic precursor-washing-dipping sulphur precursor-washing constitutes a SILAR cycle. In total, three cycles were employed to obtain a suitable amount of PbS on the TiO₂ film. The precursor (Pb(NO₃)₂, Na₂S) solution concentrations of 0.02 M, 0.04 M, 0.06 M, 0.08 M and 0.1 M were adopted to seek an appropriate concentration for the solar cells. After that, a ZnS passivation layer was deposited by two SILAR cycles while being soaked in an aqueous solution containing 0.1 M Zn(NO₃)₂ and 0.1 M Na₂S, which act as Zn²⁺ and S²⁻ sources, respectively.

Counter electrode and Electrolyte. The Cu₂S films were used as the counter electrode in this study^{14,41,42}, which were prepared on the brass foils as the following: the brass foils were immersed into 37% HCl at 70 °C for 20 min, then were washed and dried. The etched brass foils were dipped into aqueous solution containing 1 M S and 1 M Na₂S to form a Cu₂S film. The electrolyte employed in this study was composed of 1 M S and 1 M Na₂S in deionized water or mixture of deionized water and methanol with volume ratio of 7:3.

Materials and QDSC characterization. The absorption spectra were measured using a Shimadzu UV-3600 spectrophotometer. The morphology of the TiO₂ nanoparticles absorbed quantum dots was characterized by transmission electron (TEM, Tecnai G2 F20) microscopy. The electrochemical impedance spectroscopy (EIS) was carried out with use of an impedance analyzer (ZAHNER CIMP) under light intensity, 100 mW/cm². Contact angles of the electrolytes were measured with the static sessile drop method using a VCA Optima goniometer. The photovoltaic characteristics of the solar cells were evaluated using simulated AM 1.5 sunlight with an output power of 100 mW/cm² provided by a 3A grade solar simulator (Crowntech, SOL02 series). The active area of the QDSCs was 0.1256 cm² determined by a photo-mask. The current-voltage characteristics were performed using an electrochemical workstation (ZAHNER, ZENNIUM). We prepared five samples for a certain type of solar cell. So the standard deviation of the all properties is based on the statistical data of five samples measured.

References

- Graetzel, M., Janssen, R. A. J., Mitzi, D. B. & Sargent, E. H. Materials interface engineering for solution-processed photovoltaics. *Nature* **488**, 304–312 (2012).
- Kinoshita, T., Dy, J. T., Uchida, S., Kubo, T. & Segawa, H. Wideband dye-sensitized solar cells employing a phosphine-coordinated ruthenium sensitizer. *Nat. Photonics* **7**, 535–539 (2013).
- Kim, J. Y., Voznyy, O., Zhitomirsky, D. & Sargent, E. H. 25th anniversary article: Colloidal quantum dot materials and devices: a quarter-century of advances. *Adv. Mater.* **25**, 4986–5010 (2013).
- Dong, C., Li, X., Fan, X. & Qi, J. Sandwich-like Singled-Walled Titania Nanotube as a Novel Semiconductor Electrode for Quantum Dot-Sensitized Solar Cells. *Adv. Energy Mater.* **2**, 639–644 (2012).
- Tian, J. *et al.* Architected ZnO photoelectrode for high efficiency quantum dot sensitized solar cells. *Energy Environ. Sci.* **6**, 3542–3547 (2013).
- Bang, J. H. & Kamat, P. V. Solar Cells by Design: Photoelectrochemistry of TiO₂ Nanorod Arrays Decorated with CdSe. *Adv. Funct. Mater.* **20**, 1970–1976 (2010).
- Gonzalez-Pedro, V., Xu, X., Mora-Sero, I. & Bisquert, J. Modeling High-Efficiency Quantum Dot Sensitized Solar Cells. *ACS Nano* **4**, 5783–5790 (2010).
- Yu, X.-Y., Liao, J.-Y., Qiu, K.-Q., Kuang, D.-B. & Su, C.-Y. Dynamic Study of Highly Efficient CdS/CdSe Quantum Dot-Sensitized Solar Cells Fabricated by Electrodeposition. *ACS Nano* **5**, 9494–9500 (2011).
- Tian, J. J. *et al.* Enhanced Performance of CdS/CdSe Quantum Dot Cosensitized Solar Cells via Homogeneous Distribution of Quantum Dots in TiO₂ Film. *J. Phys. Chem. C* **116**, 18655–18662 (2012).
- Hines, D. A. & Kamat, P. V. Recent Advances in Quantum Dot Surface Chemistry. *ACS Appl. Mater. Interfaces* **6**, 3041–3057 (2014).
- Kamat, P. V., Christians, J. A. & Radich, J. G. Quantum Dot Solar Cells: Hole Transfer as a Limiting Factor in Boosting the Photoconversion Efficiency. *Langmuir* **30**, 5716–5725 (2014).
- Zhu, G., Pan, L., Xu, T. & Sun, Z. CdS/CdSe-Cosensitized TiO₂ Photoanode for Quantum-Dot-Sensitized Solar Cells by a Microwave-Assisted Chemical Bath Deposition Method. *ACS Appl. Mater. Interfaces* **3**, 3146–3151 (2011).
- Lee, Y. H., Im, S. H., Chang, J. A., Lee, J. H. & Seok, S. I. CdSe-sensitized inorganic-organic heterojunction solar cells: The effect of molecular dipole interface modification and surface passivation. *Org. Electron.* **13**, 975–979 (2012).
- Tian, J. J. *et al.* A highly efficient (>6%) Cd_{1-x}MnxSe quantum dot sensitized solar cell. *J. Mater. Chem. A* **2**, 19653–19659 (2014).
- Radich, J. G., Peeples, N. R., Santra, P. K. & Kamat, P. V. Charge Transfer Mediation Through Cu₂S. The Hole Story of CdSe in Polysulfide. *J. Phys. Chem. C* **118**, 16463–16471 (2014).
- Hossain, M. A. *et al.* CdSe-sensitized mesoscopic TiO₂ solar cells exhibiting >5% efficiency: redundancy of CdS buffer layer. *J. Mater. Chem.* **22**, 16235–16242 (2012).
- Lee, J.-W. *et al.* Quantum-Dot-Sensitized Solar Cell with Unprecedentedly High Photocurrent. *Sci. Rep.* **3**(1050), 1–8 (2013).
- Gonzalez-Pedro V. *et al.* High performance PbS Quantum Dot Sensitized Solar Cells exceeding 4% efficiency: the role of metal precursors in the electron injection and charge separation. *Phys. Chem. Chem. Phys.* **15**, 13835–13843 (2013).
- Scholes, G. D. & Rumbles, G. Excitons in nanoscale systems. *Nat. Mater.* **5**, 683–696 (2006).
- Schoolar, R. & Dixon, J. Optical constants of lead sulfide in the fundamental absorption edge region. *Phys. Rev.* **137**, A667 (1965).

21. Lai, L. H., Protesescu, L., Kovalenko, M. V. & Loi, M. A. Sensitized solar cells with colloidal PbS-CdS core-shell quantum dots. *Phys. Chem. Chem. Phys.* **16**, 736–742 (2014).
22. Sung, S. D., Lim, I., Kang, P., Lee, C. & Lee, W. I. Design and development of highly efficient PbS quantum dot-sensitized solar cells working in an aqueous polysulfide electrolyte. *Chem. Commun.* **49**, 6054–6056 (2013).
23. Tao, L., Xiong, Y., Liu, H. & Shen, W. Z. High performance PbS quantum dot sensitized solar cells via electric field assisted *in situ* chemical deposition on modulated TiO₂ nanotube arrays. *Nanoscale* **6**, 931–938 (2014).
24. Loidice, A. *et al.* Fabrication of flexible all-inorganic nanocrystal solar cells by room-temperature processing. *Energy Environ. Sci.* **6**, 1565–1572 (2013).
25. Lee, H. *et al.* PbS and US Quantum Dot-Sensitized Solid-State Solar Cells: “Old Concepts, New Results”. *Adv. Funct. Mater.* **19**, 2735–2742 (2009).
26. Robel, I., Subramanian, V., Kuno, M. & Kamat, P. V. Quantum dot solar cells. Harvesting light energy with CdSe nanocrystals molecularly linked to mesoscopic TiO₂ films. *J. Am. Chem. Soc.* **128**, 2385–2393 (2006).
27. Huang, X. *et al.* A flexible photoelectrode for CdS/CdSe quantum dot-sensitized solar cells (QDSSCs). *Chem. Commun.* **47**, 2664–2666 (2011).
28. Lee, Y. L. & Lo, Y. S. Highly Efficient Quantum-Dot-Sensitized Solar Cell Based on Co-Sensitization of CdS/CdSe. *Adv. Funct. Mater.* **19**, 604–609 (2009).
29. Yang, Z. *et al.* CdS/CdSe Co-Sensitized Solar Cell Prepared by Jointly Using Successive Ion Layer Absorption and Reaction Method and Chemical Bath Deposition Process. *Sci. Adv. Mater.* **4**, 1013–1017 (2012).
30. Tian, J. & Cao, G. Semiconductor quantum dot-sensitized solar cells. *Nano Rev.* **4**, 22578 (2013).
31. Cao, G. & Wang, Y. One-Dimensional Nanostructures: Nanowires and Nanorods In *Nanostructures and Nanomaterials: Synthesis, Properties and Applications*, 2nd edn (ed Reed, M.) 149–150 (World Scientific, 2011).
32. Braga, A., Gimenez, S., Concina, I., Vomiero, A. & Mora-Sero, I. Panchromatic Sensitized Solar Cells Based on Metal Sulfide Quantum Dots Grown Directly on Nanostructured TiO₂ Electrodes. *J. Phys. Chem. Lett.* **2**, 454–460 (2011).
33. Concina, I. *et al.* Modulating Exciton Dynamics in Composite Nanocrystals for Excitonic Solar Cells. *J. Phys. Chem. Lett.* **6**, 2489–2495 (2015).
34. Wang, Q., Moser, J. E. & Gratzel, M. Electrochemical impedance spectroscopic analysis of dye-sensitized solar cells. *J. Phys. Chem. B* **109**, 14945–14953 (2005).
35. Gao, R. *et al.* Interface modification effects of 4-tertbutylpyridine interacting with N3 molecules in quasi-solid dye-sensitized solar cells. *Phys. Chem. Chem. Phys.* **13**, 10635–10640 (2011).
36. Wang, Q., Moser, J. E. & Gratzel, M. Characteristics of high efficiency dye-sensitized solar cells. *J. Phys. Chem. B* **110**, 25210–25221 (2006).
37. Hoshikawa, T., Yamada, M., Kikuchi, R. & Eguchi, K. Impedance Analysis of Internal Resistance Affecting the Photoelectrochemical Performance of Dye-Sensitized Solar Cells. *J. Electrochem. Soc.* **152**, E68 (2005).
38. Tian, J. & Cao, G. Control of Nanostructures and Interfaces of Metal Oxide Semiconductors for Quantum-Dots-Sensitized Solar Cells. *J. Phys. Chem. Lett.* **6**, 1859–1869 (2015).
39. Kern, R., Sastrawan, R., Ferber, J., Stangl, R. & Luther, J. Modeling and interpretation of electrical impedance spectra of dye solar cells operated under open-circuit conditions. *Electrochim. Acta* **47**, 4213–4225 (2002).
40. Gao, R. *et al.* ZnO nanocrystallite aggregates synthesized through interface precipitation for dye-sensitized solar cells. *Nano Energy* **2**, 40–48 (2013).
41. Tian, J. J. *et al.* Microsphere Light-Scattering Layer Assembled by ZnO Nanosheets for the Construction of High Efficiency (>5%) Quantum Dots Sensitized Solar Cells. *J. Phys. Chem. C* **118**, 16611–16617 (2014).
42. Tian, J. J., Uchaker, E., Zhang, Q. & Cao, G. Hierarchically Structured ZnO Nanorods-Nanosheets for Improved Quantum-Dot-Sensitized Solar Cells. *ACS Appl. Mater. Interfaces* **6**, 4466–4472 (2014).

Acknowledgements

This work was supported by the National Science Foundation of China (51374029, 5151101345), Program for New Century Excellent Talents in University (NCET-13-0668) and Fundamental Research Funds for the Central Universities (FRF-TP-14-008C1, FRF-UM-15-074).

Author Contributions

J.J.T. contributed to the conception and design of the experiment, analysis of the data and writing the manuscript with assistance of G.Z.C. X.G.L. carried out synthesis of materials, preparation of the devices, device performance measurements and writing experimental part in the manuscript with assistance of T.S. C.B.F. carried out impedance spectroscopy. L.L.L. carried out UV-visible spectra.

Additional Information

Competing financial interests: The authors declare no competing financial interests.

How to cite this article: Tian, J. *et al.* Enhanced Performance of PbS-quantum-dot-sensitized Solar Cells via Optimizing Precursor Solution and Electrolytes. *Sci. Rep.* **6**, 23094; doi: 10.1038/srep23094 (2016).



This work is licensed under a Creative Commons Attribution 4.0 International License. The images or other third party material in this article are included in the article's Creative Commons license, unless indicated otherwise in the credit line; if the material is not included under the Creative Commons license, users will need to obtain permission from the license holder to reproduce the material. To view a copy of this license, visit <http://creativecommons.org/licenses/by/4.0/>